STUDIES OF MAGNETICS AND SUPERCONDUCTORS BY MUON SPIN ROTATION METHOD

S.G.Barsov, V.P.Koptev

Introduction

It is well known that nuclear physics methods are often used in solid state physics to study microscopic properties of matter. One of the methods called Muon Spin Rotation (μSR) is based on application of polarized muons (mainly positive charged muons μ^+) as microscopic probes implanted into the substance under investigation. Due to the fact that the angular distribution of positrons produced in the decay $\mu^+ \rightarrow e^+\nu\tilde{\nu}$ $(\tau_\mu = 2.2 \cdot 10^{-6}$ s) is asymmetric relatively to the muon spin direction, the probability to detect the decay positron within a certain solid angle depends not only on the time interval from the moment when the muon stopped inside the sample to the moment of its decay, but also on the deflection of the muon spin from the incident direction during this period. Thus, the time dependence of detected positrons reflects the behaviour of the muon polarization vector $\vec{P}(t)$.

The change of $\vec{P}(t)$ is caused by the interaction of muons and their magnetic moments with the environment. One possible way of the interaction, which is often realized in insulators and semiconductors, consists in the formation of a hydrogen-like atom – muonium (μ^+e^-). In this case, the study of the atomic hydrogen, its charge states and its chemical reactions in times comparable with τ_μ becomes possible. A great number of experiments were performed in this field. In particular, since the polarized muon channel of the PNPI proton accelerator had gone into operation in 1977, extensive studies of the muonium in semiconductors have been carried out at the High Energy Physics Division. The obtained data allowed to refine the ergodic nature of a specific charge state – "anomalous muonium". The characteristics of muonium quadrupole interaction in crystalline α-quartz were also explored. It was shown that the temperature dependence of the value and the symmetry of this interaction were caused by the muonium diffusion [1].

However, in our opinion the most significant results have been achieved in our laboratory during the last decade when the properties of metallic alloys with the competing ferro- and antiferromagnetic exchanges, as well as properties of high-T_c superconductors, were extensively studied. In these materials the muon depolarization occurs mainly due to the precession of the muon spin in local magnetic field surrounding the muon. Then determination of $\vec{P}(t)$ gives a direct way to study the type and the parameters of the local field distribution. Hence, some information concerning the microscopic properties becomes available.

Experimental technique and data treatment

All the results presented below have been obtained using the μSR-installation in the polarized muon beam at PNPI. The muon beam with the momentum of 90 to 100 MeV/c and the intensity of $\sim 10^4\mu^+$/s has about 90% polarization along the beam axis. Not less than 60% of the muons are stopped inside a pattern which usually has the shape of a disk with the diameter of 25–60 mm and the thickness of 5–10 mm (3–9 g/cm^2). The temperature of the sample is varied within the interval 4.5–320 K with the help of a helium gas-flow cryostat. In order to decrease the physical background, the cryostat has thin windows in the beam direction.

The total thickness of the windows (0.06 g/cm^2) did not exceed 2% of the sample thickness. The homogeneous external magnetic field up to 1 kOe could be applied either along ($H_{||}$) or perpendicularly ($H_\perp$) to the initial muon polarization. The experiments could be carried out without (lower than 0.05 Oe) external magnetic field as well.

The muons and decay positrons were detected by scintillators placed upstream and downstream the sample. The time resolution of the device was about 2.5 ns. The common time-measuring technique, including the control of the only one μ^+ being inside the sample during the interval 8 τ_μ, was used for the accumulation of the time dependence of decay positrons $N_e(t)$ simultaneously into two histograms with channel width of 0.5 ns and 5 ns. The dependence $N_e(t)$ may be represented as following:

$$n_e(t) = \frac{N_e(t)}{N_\mu} = \frac{N_0}{N_\mu}\left\{e^{-t/\tau_\mu}\cdot[1+a_0\cdot G(t)] + \frac{N_f}{N_0}\right\}. \tag{1}$$

Here N_μ is the total amount of μ^+'s stopped in the sample, a_0 is the experimental asymmetry coefficient. The parameters a_0, N_0/N_μ, and N_f/N_0 depend on the initial muon polarization, the efficiency of detectors, and the background conditions. They were measured in control experiments and have the following typical values: $a_0 = 0.25$–0.30, $N_0/N_\mu = 0.04$–0.06, and $N_f/N_0 \simeq 10^{-3}$. The only parameter in (1) related to $\vec{P}(t)$ is the function $G(t)$ which in our experimental geometry is the projection of $\vec{P}(t)$ on the direction of the initial muon polarization. Taking into account that the muons are almost randomly stopped anywhere in the sample volume and that the local fields $\vec{h}$ may have arbitrary values and directions, the function $G(t)$ might be presented as:

$$G(t) = \int\left[\frac{h_z^2}{h^2} + \frac{h_x^2+h_y^2}{h^2}\cdot\cos(\gamma_\mu h t)\right]W(\vec{h})d\vec{h}. \tag{2}$$

Here Z-axis is directed along the muon beam (the initial muon polarization), $W(\vec{h})$ is the distribution of local magnetic fields, and $\gamma_\mu = 2\pi\cdot 13.55$ kHz/Oe is the muon gyromagnetic ratio. Generally speaking, it is possible to determine $W(\vec{h})$ from the experimental data. But usually some physical model is still necessary for interpretation of the results. Such a model is commonly used to fix the type of the $W(\vec{h})$ and $G(t)$ dependences, and then the comparison with the experimental data is done using the known least-squares procedure.

However, sometimes already the simplest analysis of $N_e(t)$ allows to obtain an essential information. Indeed, if the characteristic time of the local fields variation τ_c is much bigger than τ_μ, then the first term in (2) is almost independent of time. Hence, the ratio of magnitudes of the first and the second (oscillating) terms is defined by the angular distribution of $\vec{h}$ only. This case is usually realized for magnetically ordered states below the magnetic transition temperature. Speaking to the point, this feature was used at PNPI for development of a method for studies of the magnetic texture in electrotechnical steels [2]. The texture is known to effect the efficiency of electric current transformers. For the isotropic angular distribution of quasistatic local fields, the function $G(t)$ has the definite coefficients:

$$G(t) = \frac{1}{3} + \frac{2}{3}\int\cos(\gamma_\mu h t)W(h)dh. \tag{3}$$

The second term is determined by the distribution of local magnetic field values, some concrete cases will be considered later. Now it is worth pointing that it is sensitive to the relation between the first $< h >= B$ and the second $< h^2 - < h >^2 >= \Delta^2$ moments of $W(h)$.

If $B \gg \Delta$, there are slow damping oscillations with the frequency $\gamma_\mu B$, while the damping rate significantly rises with increasing Δ/B.

The effect of fast variations of $\vec{h}$ ($\tau_c < 10^{-5}$ s) depends on the value of $\gamma_\mu h\tau_c$. At $\gamma_\mu h\tau_c \ll 1$ the local magnetic fields have almost no influence on the muon polarization behaviour. This, for instance, leads to a very slow depolarization of muons in the paramagnetic state where $\tau_c \simeq 10^{-12}$ s. For the intermediate interval 10^{-10} s $< \tau_c < 10^{-5}$ s the following parametrization of $G(t)$ may be usually applied excluding a narrow region around the transition temperature:

$$G(t) = G_s(t) \cdot G_d(t); \qquad G_d(t) = \exp(-\lambda t), \tag{4}$$

The function $G_d(t)$ describes the muon relaxation caused by the dynamics of the local fields, while $G_d(t)$ corresponds to the muon depolarization in the quasistatic case (see (2),(3)).

Study of magnets with competing magnetic exchanges

The specific feature of such systems is the exchange interaction between the neighbouring magnetic atoms which has random value and sign. Although these materials may have a crystalline lattice, they are generally considered as disordered magnets to distinguish them from the magnets with definite parameters of the exchange interaction. The magnetic state of the latter systems can be described using only one order parameter – the magnetization $\vec{M}$. But for disordered magnets another order parameter – the dispersion of the local magnetization Q – must be involved (S.F.Edwards and P.V.Anderson, 1975). It has been theoretically found that a nonmagnetic substance contaminated by a small amount (about 1%) of magnetic atoms (so-called dilute system) with decreasing of the temperature could exhibit the transition from the paramagnetic state ($\vec{M} = 0, Q = 0$) into the disordered magnetic phase with $\vec{M} = 0$ and $Q \neq 0$ called spin glass – SG. The further investigation (S.Kirkpatrick and D.Scherington, 1978) has shown that this type of phase transition might also take place in materials with high concentrations of the magnetic component (concentrated systems). Moreover, it has been predicted that the transition into the low temperature SG phase might occur not only from the paramagnetic (P) state directly, but also through an intermediate state with a long range magnetic order (LRMO) and $\vec{M} \neq 0$. In the last case, the order parameter Q may contain at least two components: longitudinal $Q_\parallel$ and transverse $Q_\perp$ relatively to $\vec{M}$. Hence, the LRMO phase should be considered either as a collinear ordered state ($Q_\parallel \neq 0, Q_\perp = 0$) or as a superposition of LRMO along the direction of $\vec{M}$ and the spin glass order in the perpendicular plane ($Q_\parallel \neq 0, Q_\perp \neq 0$) called sometimes the asperomagnetic state. Similar to SG the asperomagnetic phase must be nonergodic. Hence, some transition from an ergodic LRMO state to a nonergodic one may occur within the intermediate LRMO phase. Thus, a rich spectrum of magnetic phases may be expected to appear in the disordered magnets. But which of them could be realized under different conditions should be answered by experimental investigations, of course. However, while in 1985 the properties of the dilute systems (such as $Cu_{1-x}Mn_x$ with $x < 0.05$) have been quite well studied using different methods, many basic questions on the concentrated systems remained unclear yet.

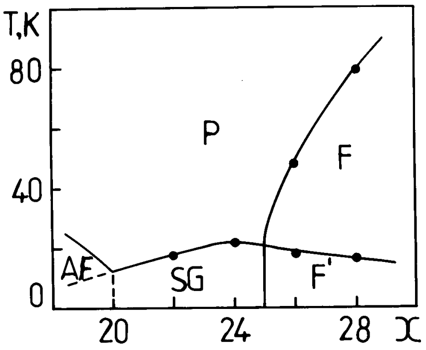

Fig. 1. The magnetic phase diagram of $Fe_{82-x}Ni_xCr_{18}$ alloy. P, F, AF denote the para-, the ferro- and the antiferromagnetic phases. SG, F' – the spinglass-like phases.

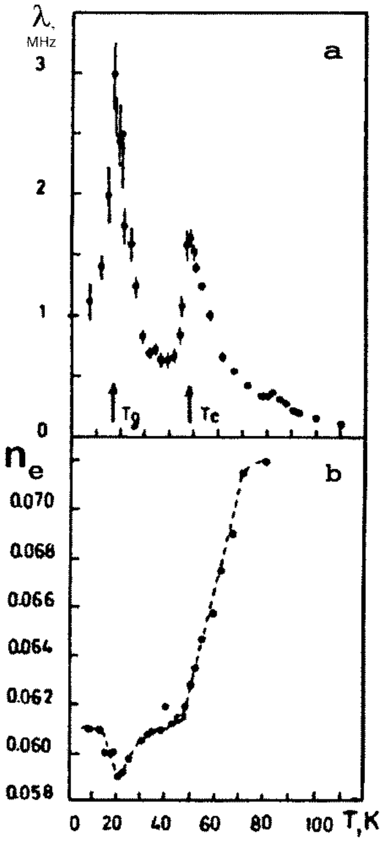

Fig. 2. Temperature dependences of the dynamical relaxation rate $\lambda(T)$ (a) and of the integral positron yield (b) in $Fe_{54}Ni_{26}Cr_{18}$.

The alloy $Fe_{82-x}Ni_xCr_{18}$ explored by us [3,4] has the typical for such systems magnetic phase diagram (Fig. 1). According to the data published at that time, the properties of the low-temperature phase formed both from the P phase ($20 \leq x \leq 25$) and from the intermediate ferro- ($x > 25$) or antiferromagnetic ($x < 20$) phases were very similar to the specific properties of SG. But it has not been found out if the phase had the same magnetic structure within the concentration region, as well as if its structure was the same as SG in dilute systems. The appearance of the asperomagnetic state within the intermediate phase was an open question too. It must be pointed out that the investigations of the intermediate phase using the neutron scattering and electromagnetic techniques have faced a number of difficulties which limited the capability of the methods. Therefore, the temperatures of transition to the low temperature phase have not been unambiguously determined yet.

The application of the μSR method allowed to clear up the situation. The point is that significant fluctuations of the local magnetic fields appear near the transition temperature. They may be caused either by the spontaneous correlations of the atomic spins (P $\rightarrow$ F,AF) or by the changing of the magnetic order (F,AF $\rightarrow$ SG). The local field fluctuations lead to the dynamical relaxation of the muon polarization (see (4) and Fig. 2). The maximum of the dependence $\lambda(T)$ corresponds to the temperature below which a new magnetic phase appears, i.e. the temperature of magnetic phase transition. The dependence $\lambda(T)$ shown in Fig. 2a was typical for all the studied samples with $x < 20$ and $x > 25$. The first (high temperature) peak corresponds to the transition P $\rightarrow$ F(AF). The second peak reflects the transition to the spin glass state. This is obvious from the temperature dependence of the integral yield of the decay positrons measured at $H = 0$ (Fig. 2b):

$$n_e = N_e/N_\mu = N_\mu^{-1} \int N_e(t)dt. \tag{5}$$

The integration is done over the interval t = 0–5 τ_μ. As it follows from expressions (1)–(5), at $H = 0$ the value of n_e is maximal ($n_e^{\max}$) in the paramagnetic phase because without the muon depolarization $G(t) = 1$ for the used geometry of the experiment.

At large value of $H_\perp$ the positron yield has a minimum value $n_e^{\min}$ (because $G(t) = \cos(\gamma_\mu H t)$ and $\gamma_\mu H \tau_\mu \gg 1$) and corresponds to the case of complete depolarization. Thus, the decrease of n_e measured at $H = 0$ with lowering the temperature directly indicates the appearance of spontaneous local magnetic fields inside the sample. In magnets these fields are usually so large that n_e can differ from $n_e^{\min}$ only due to longitudinal field components h_z (see (2)). If the local fields are quasistatic, then in the nontextured polycrystalline sample the value of n_e must be close to $n_e^{\min}+1/3\cdot(n_e^{\max}-n_e^{\min})$ for any kind of the magnetic order. But fluctuations of the fields decrease this value. Hence, Fig. 2 shows that there is a transition from one magnetic phase to another in the vicinity of $T \simeq 20$ K. This original application of the μSR method developed at PNPI [5] is quite effective for the determination of the magnetic transition temperature, as well as for the search for irreversible phenomena. It also allows to choose such external conditions at which the main and the most complicated goal of the μSR experiment (consisting in the measurement of the local field distribution) could be achieved in the most effective way.

Another important point is the correct determination of the type of $G(t)$. This problem has been considered in many works but all of them concerned either the ordered magnets or the dilute spin glasses with $\vec{M} = 0$. Our investigation has required to choose an appropriate $G(t)$ for the disordered magnetic state with $\vec{M} \neq 0$. This has been done in our laboratory [6] in the framework of the phenomenological approach based on expression (2). The following analytical expression describing the muon polarization behaviour in a disordered state with $B \neq 0$ and $\Delta_{||} = \Delta_{\perp} = \Delta$ has been obtained:

$$G(t) = \frac{1}{3} + \frac{2}{3}\left[\cos(\gamma_\mu Bt) + (\gamma_\mu \Delta t)^\alpha \frac{\sin(\gamma_\mu Bt)}{\gamma_\mu Bt}\right] \exp(-\frac{(\gamma_\mu \Delta t)^\alpha}{\alpha}). \tag{6}$$

Here the parameter α is equal either to 1 for the Lorentzian type of the local field distribution or to 2 for the Gaussian type. It is easy to see that function (6) turns into the previously found $G(t)$ for the collinear ordered state or for the dilute spin glass in the limits $\Delta_\perp \to 0$ and $B \to 0$, respectively. The application of $G(t)$ from (6) to the experimental data has shown that the intermediate phase at $x > 25$ was the asperomagnetic state. The most obvious difference between this state and the case of the collinear magnets was observed in experiments with the external magnetic field (Fig. 3). It is interesting that in the alloy under investigation the formation of the asperomagnetic state occurred, perhaps, just after the transition into the ferromagnetic phase.

The measured temperature dependences of B and Δ (Fig. 4) , which are related to the mentioned above order parameters $\vec{M}$ and Q, indicated that the magnetic structure of the low temperature phase at $x > 25$ was significantly different from the structure of SG observed in the dilute magnets. At the same time, below the second transition, not only Δ but also B was found to be increasing. This indicates that some short-range ferromagnetic order is remained for $x > 25$ down to 5 K. But in the samples with $x = 22$ and $x = 24$ the low temperature phase resulted in the transition from the paramagnetic state was found to have $B \simeq 0$. The temperature dependences of Δ for these samples were very similar to the expected temperature behaviour of Q in the dilute SG. The only specific feature of the SG phase at $20 \leq x \leq 25$ was the local field distribution of the Gaussian type, while the Lorentzian type distribution has been observed in the dilute spin glasses. The temperature dependences of the magnetic correlation radii R_c determined by the comparison of the μSR with the neutron depolarization data for the samples with $x = 24$ and $x = 26$ were also different [7]. For $x = 24$ the value of R_c below the transition reached zero with decreasing the temperature, but for $x = 26$ after the transition F $\to$ SG R_c changed its value from 1000 Å to 100 Å only.

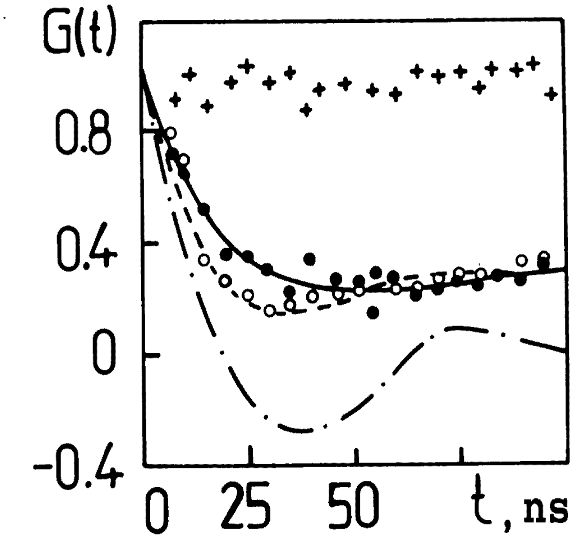

Fig. 3. Functions $G(t)$ in $Fe_{56}Ni_{26}Cr_{18}$ at $H = 0$ ($T = 95$ K (crosses) and $T = 40$ K (solid circles) as well as at $H_{\perp} = 350$ Oe, $T = 40$ K (open circles). The solid curve represents the fit with (6) for $H = 0$. The obtained B and Δ were used for the calculation of $G(t)$ at $H_{\perp} = 350$ Oe in the asperomagnetic (dashed curve) and in the collinear (dash-dotted curve) states.

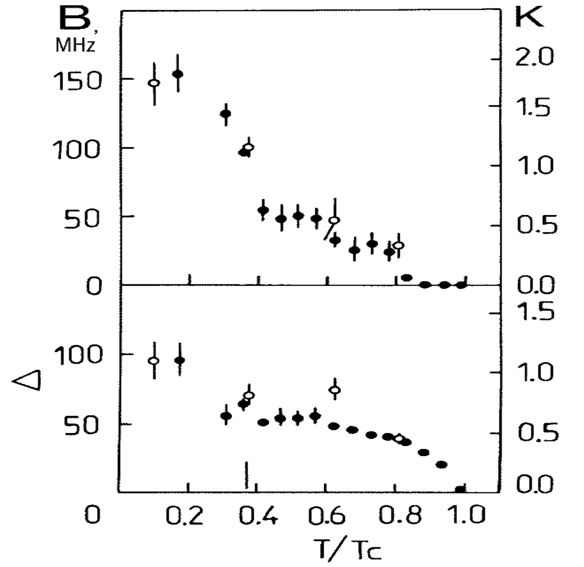

Fig. 4. Temperature dependences of B and Δ at $H = 0$ obtained with (6) for $Fe_{56}Ni_{26}Cr_{18}$ (solid circles) and $Fe_{54}Ni_{28}Cr_{18}$ (open circles) samples.

The investigation of the samples with $x = 16$ and $x = 18$ has shown [7] that the asperomagnetic phase preceding the transition to the low temperature phase took place in AF phase too. In this case the structure of the low temperature state was found to be more complicated. The coexistence of both the spin glass order with $B \simeq 0$ and the asperomagnetic phase with $B \neq 0$ was observed there. The explanation of this feature of the antiferromagnetic region of the magnetic phase diagram is not clear at present.

Thus the μSR studies not only confirmed but also complemented the theoretical predictions mentioned above. The only difference was no significant dynamics of the local fields, which could indicate the formation of the nonergodic state, found within the LRMO phase. With the assumption that such dynamics could be camouflaged by fluctuations due to relatively close spaced transitions P $\rightarrow$ F(AF) and F(AF) $\rightarrow$ SG, we have continued to study the effect with another concentrated system – the alloy $Fe_xMn_{1-x}Pt_3$. The magnetic phase diagram of the material contained the tricritical point for P, F, and AF states at $x = 0.66$. A mixed phase exhibiting both the ferro- and antiferromagnetic ordering has been found at $0.5 < x < 0.6$ below the ferromagnetic state with the neutron diffraction method. A weak irreversibility of the magnetic susceptibility indicating the possible presence of a nonergodic phase was also observed below T_c.

The samples of the alloy with $x = 0.45$; 0.55; 0.60; 0.65, and with $x = 0.8$ have been studied using the μSR method [8,9]. It was shown that there was only one phase transition P $\rightarrow$ AF in the sample with $x = 0.8$, while at $x < 0.66$ the temperature dependence of the dynamical relaxation rate measured at $H = 0$ demonstrated three maxima. The dependence $\lambda(T)$ presented in Fig. 5 was typical for all the samples. It is clearly seen that the strong spin dynamics appears not only in the transitions to the ferromagnetic (T_c) and to the mixed (T_N) states but also within the F–phase. The position of the third peak (T_A) approximately corresponds to the temperature below which the mentioned irreversibility of the susceptibility arises. One may assume that the formation of the nonergodic LMRO state takes place near the temperature T_A. But the large dynamical relaxation rate and the small size of the samples did not allow us to determine the distribution of the quasistatic local fields. Therefore, the field dependence of T_A has been measured only. The matter is that, according to the theoretical predictions (M.Gabay and G.Toulouse, 1981), the temperature of the transition into the nonergodic LMRO state should have a special dependence on the external magnetic field value. For Heizenberg's magnets this dependence in the (H, T)–diagram is presented by the Gabay–Toulouse line, while for Ising's magnets it follows the Almeida–Thouless line. In our case the dependence $T_A(H)$ rather corresponds to the former case. Hence, the nonergodicy in the system under investigation is caused, perhaps, by the freezing of transverse components of the magnetic moment.

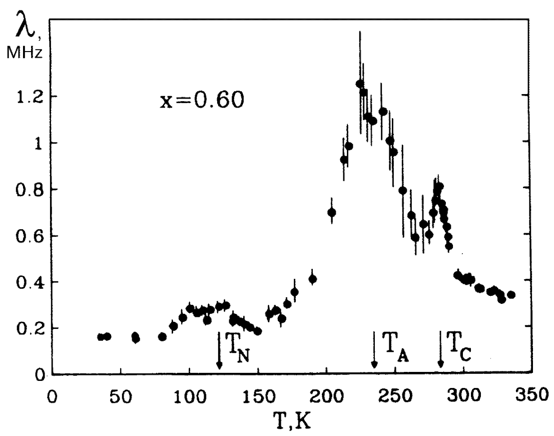

Fig. 5. The temperature dependence of the dynamical muon relaxation rate in $Fe_{0.6}Mn_{0.4}Pt_3$ at $H = 0$. Transitions into the ferromagnetic (T_c), the mixed (T_N) and the nonergodic (T_A) phases are shown by arrows.

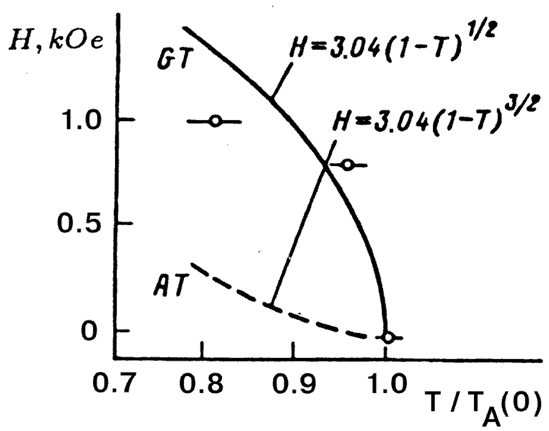

Fig. 6. The field dependence of T_A in $Fe_{0.6}Mn_{0.4}Pt_3$. Gabay–Toulouse (GT) and Almeida–Thouless (AT) dependences are presented by the solid and the broken curves, respectively.

Study of magnetism and high temperature superconductivity in oxide compounds

. According to the BCS theory, it is unlikely that the weak electron-phonon interaction could provide the superconductivity above 30–40 K. Therefore, the discovery of the high-T_c superconductivity (HTSC) found since 1986 in a number of oxide compounds has stimulated the search for novel mechanisms of charge carrier coupling. One of the approaches is based on the assumption that magnetic correlations of the copper atom spins in CuO_2 planes could play a significant role in the coupling process (V.J.Emeri, 1987). The fact that all the high-T_c superconducting materials are transformed into the antiferromagnetic insulators by changing their chemical composition makes the approach to be reasonable enough. For instance, during 1987 it has been established that in the famous compound $La_{2-x}(Sr,Ba)_xCuO_4$ (which is the superconductor at $x = 0.15$–0.20 with $T_c \simeq 40$ K) T_c lowered towards zero with decreasing of Sr (or Ba) concentration. After that the antiferromagnetic order of the copper spins was observed to appear at $x < 0.05$–0.07. The experimental magnetic phase diagram of the material was determined to be in good agreement with the theoretical one (A.Aharoni et al., 1988) which predicted the presence of the spin glass state near $x = 0.05$–0.07. The similar concentration transition has been also found near $x = 0.4$–0.5 in another compounds – $YBa_2Cu_3O_{6+x}$ ($0\leq x \leq 1$, $T_c \simeq 90$ K at $x \simeq 1$). But the last material discovered in the beginning of 1987 has not been explored in detail at that time.

The careful investigation of properties of the $YBa_2Cu_3O_{6+x}$ compound in dependence on the oxygen concentration has been the main goal of our study of the high-T_c superconducting oxides [10]. Special attention has been paid to the region $0.3\leq x \leq 0.6$ where coexistence of the superconductivity with some kind of the copper magnetism was expected. The dependences $n_e(T)$ (see (5)) presented in Fig. 7 show no influence of the atomic magnetic moments on the muon polarization behaviour up to 4.6 K for $x > 0.60$. Hence, the correlation time of the electron spins does not exceed 10^{-12}–10^{-9} s within this concentration region. The small difference of n_e from $n_e^{\max}$ was caused by weak internal magnetic fields (~ 5 Oe) produced by the nuclear magnetic moments of the copper atoms. It should be pointed out that the transition into the superconducting state ($T_c \simeq 60$ K for $x = 0.60$) did not effect the muon depolarization within the experimental errors of 0.3% as measured at $H = 0$.

But for $x \leq 0.50$ the significant decrease of n_e was observed below some temperature. So, the transitions into the magnetic phase took place there, while the samples with $x > 0.40$ were still superconducting. The magnetic phase was determined from neutron diffraction experiments to be the long-range antiferromagnetic state with $T_N > 300$ K for $x \leq 0.3$. At $T \ll T_N$ the local magnetic fields were quasistatic and isotropically oriented due to the granular structure of the sample. The fact that with decreasing the temperature n_e achieved the value $n_e^{\min} + 1/3(n_e^{\max} - n_e^{\min})$ for all the samples with $x \leq 0.42$ indicated that at 4.6 K the magnetic phase occupied not less than 95% of the sample volume. This conclusion was also confirmed by the analysis of $G(t)$ measured at $H = 0$ and $T \ll T_N$. It was found that within the interval $0.2 \leq x \leq 0.42$ the dispersion of spontaneous local fields was increased by a factor of 4 with x increasing, while the change in the mean value of the fields was not more than 20%. Thus, the long-range magnetic order was continuously destroyed while approaching the region of superconductivity ($x > 0.40$). However, the functions $G(t)$ measured at $T = 4.6$ K for all the samples with $x \leq 0.42$ correspond rather to the case of the collinear magnet than to the asperomagnetic or SG phases. Besides, no irreversible phenomena which could point on the nonergodic nature of the magnetic state were found.

Unlike to the case $H = 0$, the muon polarization behaviour in the external magnetic field $H_\perp$ is significantly changed as a result of transition from the "normal" (paramagnetic) phase to the superconducting one. When the sample was cooled in the constant $H_\perp$ (so-called procedure FC), the following approximation of $G(t)$ was used:

$$G(t) = a_o^{-1} \left[a \cdot e^{-\sigma^2 t^2} \cos(\gamma_\mu B t) + a_N \cdot e^{-\sigma_N^2 t^2} \cos(\gamma_\mu H t) \right] . \tag{7}$$

Above the transition temperature ($T > T_c$) $a/a_o = 0$ and the slow damping ($\sigma_N \simeq 0.08 \cdot 10^6$ s^{-1}) precession with the frequency determined by the value of H took place. But below T_c a significant increase of the dispersion of local fields ($\sigma > \sigma_N$), as well as a decrease of their mean value ($B < H$), appeared with the sample cooling due to formation of the vortex structure of the magnetic flux (HTSC is the II-type superconductivity). The measured dependences $\sigma(T)$ and $B(T)$ have shown that the superconducting transition took place in all the samples with $x > 0.40$. Its temperature T_c increased from 35 K for $x = 0.42$ to 90 K for $x = 0.95$ in a good agreement with the results obtained by other methods. In spite of broadening the transition width for $x < 0.55$, the relative volume of the superconducting phase determined from the value a/a_o (see (7)) at $T = 15$ K achieved 95% of the sample volume for $x \geq 0.45$ and was not less than 40% of it for $x = 0.42$ (Fig. 8). But the μSR-measurement of the superconducting phase volume at 4.6 K in the samples with $x < 0.50$ was too difficult because the inhomogeneity of

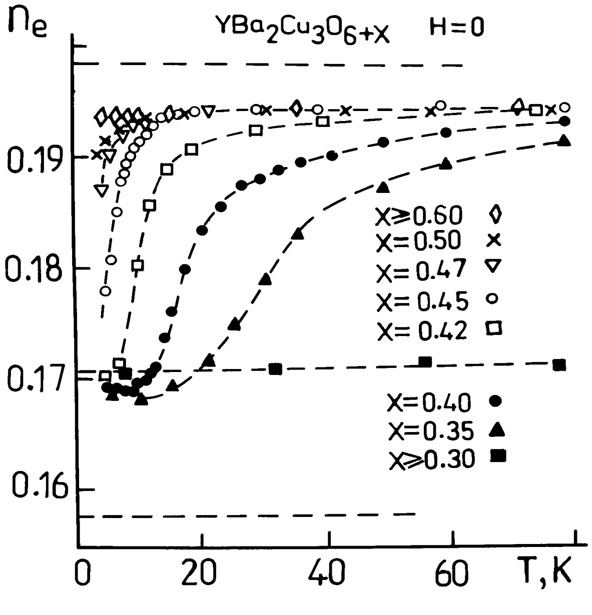

Fig. 7. Temperature dependences of the integral positron yield at $H = 0$ in ceramics $YBa_2Cu_3O_{6+x}$ with different oxygen concentrations. The broken straight lines correspond to n_e^{max} (upper), n_e^{min} (lower) and to $n_e^{min} + 1/3(n_e^{max} - n_e^{min})$ (middle).

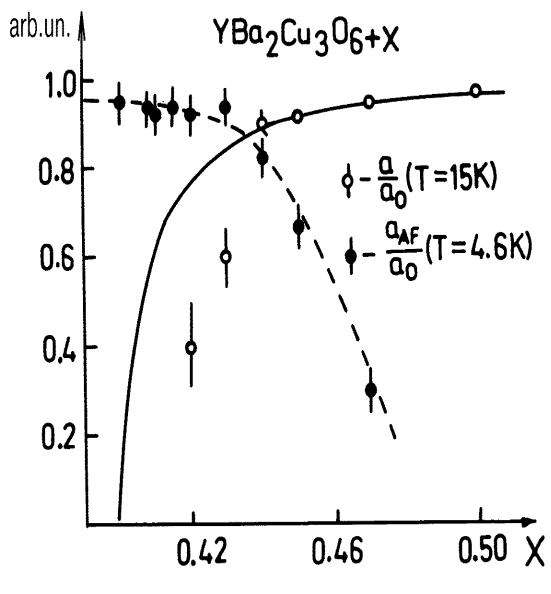

Fig. 8. The relative volume of samples occupied by the superconducting phase at 4.6 K (the solid line, determined from the susceptibility measurements) and at 15 K (open circles, from μSR data) as well as by the magnetic phase at 4.6 K (solid circles, determined by μSR). The broken curve is drawn to guide eye.

spontaneous local fields in the magnetic state much exceeded the dispersion due to the vortex structure. Therefore, the magnetization of the samples in the alternating external magnetic field of 0.25 Oe, as compared with the magnetization of the lead sample having the same shape and size has been measured for this purpose. It must be pointed that the results of both methods have coincided at $T = 15$ K.

As seen from Fig. 8, the relative volumes of both the magnetic and the superconducting phases at $T = 4.6$ K were not less than 70–80% of the sample volume for $0.41 \leq x \leq 0.43$. The careful studies of the nonsuperconducting sample with $x = 0.40$ and the superconducting one with $x = 0.42$ carried out under the same conditions have shown that the magnetic ordering had the same structure in both the samples. Besides, it has been found out that there was no any significant macroscopic inhomogeneity of the oxygen concentration through the volume of both samples. Hence, at least in the interval $0.41 \leq x \leq 0.43$ the coexistence of the superconductivity and the magnetism must be realized within a spatial length not more than several elementary cells.

Another remarkable feature of HTSC is the strong anisotropy caused, perhaps, by the layered crystalline structure of the oxide compounds. Indeed, the charge transport capability of high-T_c superconductors are known to be much larger along atomic planes (the crystallographic plane ab) than perpendicularly to them (along the axis c). It is assumed that the two-dimensional nature of HTSC can lead to a rise of T_c. That is why along with the compound $YBa_2Cu_3O_{6+x}$ the textured sample of another high-T_c superconductor $Bi_2Sr_2CaCu_2O_8$ with $T_c \simeq 90$ K but larger separation of CuO_2-planes has been studied [11].

Presented in Fig. 9 temperature dependences of the local field dispersion below T_c have been measured using FC procedure with $H \gg H_{c1}$. This way provided the formation of the most regular vortex structure. The parameter σ was theoretically shown (W.Barford and J.M.F.Gann, 1988) to be directly related to the magnetic field penetration depth δ which is one of basic microscopic characteristics of superconductivity:

$$\sigma(T) = \text{const} \cdot \delta^{-2}(T). \tag{8}$$

Here $\delta = \delta_{ab}$ at $H \parallel c$ and $\delta = (\delta_{ab} \cdot \delta_c)^{1/2}$ at $H \perp c$. In the nontextured granular superconductor $\delta \simeq 1.23 \cdot \delta_{ab}$. The temperature dependence of δ measured by μSR in both ceramic and single crystal samples of $YBa_2Cu_3O_{6+x}$ was found to be well described by the expression $\delta(T) = \delta(0) \cdot [1 - (T/T_c)^4]^{-1/2}$ which was valid for isotropic "low temperature" superconductor too. But in the bismuth based high-T_c superconductors $\delta(T)$ rather follows the dependences calculated in the assumption of a strong coupling (J.Rammer, 1988). It is interesting that $\delta_{ab}(T)$ corresponded to the "clean" limit, when the free length of carriers was much more than the coherent length, while along c-axis values of both the lengths were not significantly different. This result shows that in spite of the small coherent length value in high-T_c superconductors (20–30 Å), the "dirty" limit is possible. Therefore, the hypothesis of the universal linear relation between T_c and the carrier concentration (J.Uemura et al., 1988) based on the consideration of the "clean" limit case only should be revised.

The two-dimensional nature of HTSC leads, perhaps, to another unusual phenomenon called a giant creep of magnetic flux. This looks like large mobility of the magnetic flux inside the sample occurring after the external magnetic field was changed at $T \ll T_c$. In order to investigate it, we have used the textured sample of $Bi_2Sr_2CaCu_2O_8$. The external magnetic field H either was switched off after the cooling of the sample from $T_c < T$ to a certain temperature below T_c (procedure FrFC) or was applied after the sample has been cooled at $H = 0$ (procedure

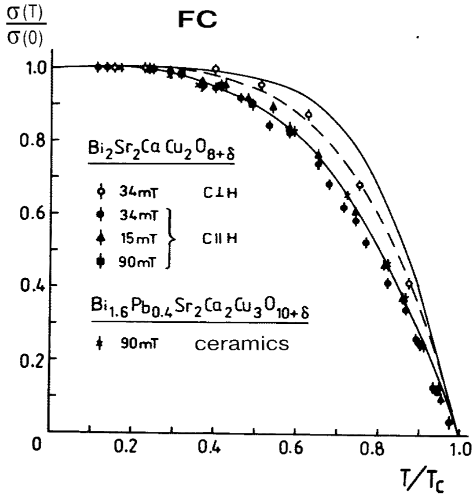

Fig. 9. Temperature dependences of the local field dispersion in the vortex structure. The broken curve shows the dependence $1-(T/T_c)^4$. Solid curves represent calculations for the strong coupling case in "dirty" (upper) and "clean" (lower) limits.

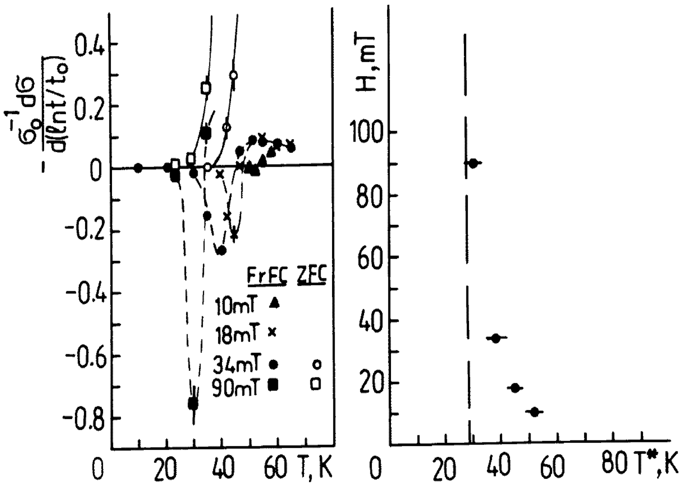

Fig. 10. The rate of changing the local field dispersion in the gradiential magnetic flux as a function of temperature (on the left) and the magnetic field dependence of melting temperature T^* of the vortex structure (on the right), the broken line is the linear extrapolation of data obtained by P.L.Gammel et al. (1988) into the low field region.

ZFC). It was found that at $T < 30$ K in result of both the procedures the structure of the magnetic flux inside the sample could be explained by the critical state model. Namely, the initial distribution of local fields, which took place before the changing of H, remained within a part of the sample volume, while a strong inhomogeneity of the fields appeared within the rest of the volume due to the gradient of the magnetic flux. The parameters of the gradiential flux, as well as its volume, have remained almost unchanged during several hours after the external field has been changed. Hence, the case of a strong pinning of vortexes has been realized at $T < 30$ K. However, the strong logarithmic time dependences of the gradiential flux parameters have appeared at $T > 30$ K above some temperature T^* (Fig. 10).

The analysis of the obtained data has shown that it was impossible to explain them in the framework of the thermally activated creep model only. For instance, according to this model the volumes occupied by the gradiential magnetic flux after both FrFC and ZFC at the same temperature should be equal. This actually takes place at $T < 30$ K. But near T^* after FrFC the mobility of the magnetic flux occurred within those areas of sample, in which, according to ZFC data, a significant gradient of the magnetic flux must be absent. In our opinion, the phenomenon of the giant creep in high-T_c superconductors is rather caused by the "melting" of the vortex structure, which is due, possibly, to the two-dimensional nature of HTSC (D.S.Fisher, 1980).

References

[1] *S.G.Barsov, A.L.Getalov, V.A.Gordeev, S.P.Kruglov, L.A.Kuz'min, S.M.Mikirtychyants, G.V.Shcherbakov, V.G.Baryshevskii, S.A.Kuten, V.I.Rapoport.* // Hyperfine Interact., 1986. V.32. P.631.

[2] *S.G.Barsov, A.L.Getalov, V.A.Gordeev, S.P.Kruglov, L.A.Kuz'min, S.M.Mikirtychyants, G.V.Shcherbakov, V.Yu.Miloserdin.* // Izvestiya Akademii Nauk SSSR, 1982. V.46. P.643.

[3] *S.G.Barsov, A.L.Getalov, S.L.Ginsburg, V.P.Koptev, S.P.Kruglov, L.A.Kuz'min, S.V.Maleev, E.I.Maltsev, S.M.Mikirtychyants, N.A.Tarasov, G.V.Shcherbakov, V.G.Grebinnik, V.N.Duginov, A.B.Lazarev, V.G.Olshevski, S.N.Shilov, V.A.Zhukov, I.I.Gurevich, B.F.Kirillov, A.I.Klimov, B.A.Nikolski, A.V.Pirogov, A.N.Ponomarev, V.A.Suetin.* // Hyperfine Interact., 1990. V.64. P.415.

[4] *G.A.Takzei, S.G.Barsov, M.V.Gavrilenko, A.L.Getalov, I.V.Golosovskii, Yu.P.Grebenyuk, F.M.Dvoeglasov, V.P.Koptev, L.A.Kuz'min, S.M.Mikirtychyants, V.P.Plakhtii, F.B.Surzhenko, I.I.Sych, V.P.Kharchenkov, G.V.Shcherbakov.* // Zh. Eksp. Teor. Fiz., 1991. V.100. P.1536.

[5] *S.G.Barsov, A.L.Getalov, V.P.Koptev, L.A.Kuz'min, S.M.Mikirtychyants, N.A.Tarasov, G.V.Shcherbakov.* Preprint LNPI–1312, Gatchina, 1987. 29p.

[6] *V.P.Koptev, N.A.Tarasov.* Preprint LNPI–1313, Gatchina, 1987. 20p.

[7] *V.P.Koptev, S.V.Maleev, N.A.Tarasov.* Preprint LNPI–1379, Gatchina, 1988. 17p.

[8] *S.G.Barsov, G.P.Gasnikova, A.L.Getalov, V.P.Koptev, S.A.Kotov, L.A.Kuz'min, A.Z.Menshikov, S.M.Mikirtychyants, G.V.Shcherbakov.* // Pis'ma Zh. Eksp. Teor. Fiz., 1993. V.57 P.651.

[9] *S.G.Barsov, G.P.Gasnikova, A.L.Getalov, V.P.Koptev, S.A.Kotov, L.A.Kuz'min, A.Z.Menshikov, S.M.Mikirtychyants, G.V.Shcherbakov.* // Pis'ma Zh. Eksp. Teor. Fiz., 1994. V.60 P.784.

[10] *S.G.Barsov, A.A.Vasilyev, A.L.Getalov, V.P.Koptev, L.A.Kuz'min, S.M.Mikirtychyants, G.V.Shcherbakov, V.I.Kulakov, R.K.Nikolaev, N.S.Sidorov, V.K.Fedotov, V.M.Mukovskii, A.S.Nigmatulin, S.E.Strunin.* // Sverkhprovodimost', 1992. V.5. P.464.

[11] *S.G.Barsov, A.L.Getalov, V.P.Koptev, I.Ya.Korenblitt, L.A.Kuz'min, S.M.Mikirtychyants, G.V.Shcherbakov, N.S.Sidorov, S.G.Karabashev, A.S.Nigmatulin.* // Sverkhprovodimost', 1992. V.7. P.1037.